Hot spot visual evaluation of breakdown locations in ATLAS18 ITk strip sensors and test structures

A. Fournier[a,b,*], V. Fadeyev[c], J. Fernandez-Tejero[a,b], B. Hommels[d], C. Jessiman[e], J. Keller[e], C. Klein[e], T. Koffas[e], S. O'Toole[a,b], J. Osieja[a,b], L. Poley[a,b], E. Staats[e], B. Stelzer[a,b], M. Ullan[f], Y. Unno[g]

[a] *Simon Fraser University, 8888 University Dr, Burnaby, V5A 1S6, ON, Canada*
[b] *TRIUMF, 4004 Wesbrook Mall, Vancouver, V6T 2A3, BC, Canada*
[c] *University of California (SCIPP), 1156 High Street , Santa Cruz, 95064, CA, US*
[d] *University of Cambridge, The Old Schools, Trinity Ln, Cambridge, CB2 1TN, UK*
[e] *Carleton University, 1125 Colonel By Dr, Ottawa, V6T 2A3, ON, Canada*
[f] *Instituto de Microelectronica de Barcelona (IMB-CNM CSIC), Campus UAB-Bellaterra, Carrer dels Til·lers, 08193, Barcelona, Spain*
[g] *High Energy Accelerator Research Organization (KEK), 1-1 Oho, Tsukuba, 305-0801, Ibaraki, Japan*

ATL-ITK-PROC-2024-003
12 February 2024

Abstract

An important characteristic of silicon-based particle detectors, such as those used for the forthcoming ATLAS ITk upgrade for the HL-LHC, is the leakage current. This characteristic is evaluated in the quality control stage of the new ITk strip sensors by performing an IV measurement, where the sensors are biased up to $-700\ V$, typically showing low and stable leakage current. However, some sensors can exhibit a sudden leakage current increase during the IV measurement, so-called early breakdown, making the sensor unusable.

The analysis of these early breakdown conditions typically consists of visual inspection of the sensors using a microscope, as often this is caused by physical damage, such as a deep scratch, chipping on the edges of the sensor, or other damage. But up to this point, the association of the observed damage with the early breakdown is not definitive. Rather, this is an association by correlation, due to the limits of verification by observation with standard equipment.

*Corresponding author
Email address: afournie@sfu.ca (A. Fournier)

A hot spot imaging setup has proven to be a valuable diagnostic tool to identify and understand these early breakdown conditions and elaborate on former understandings of these emissions. The regions responsible for the breakdown can be properly located by imaging the near infra-red light emissions produced by them in breakdown conditions. These regions of interest can also be imaged at magnification to evaluate the more precise structure of the breakdown to better understand the damage. The regions discovered, which have improved our understanding of breakdown damage and its symptoms, include scratches, chipping, static charge buildup and fabrication defects in the ATLAS18 strip sensors and test structures.

Keywords: ATLAS, silicon strip sensors, hot spot, thermal imaging, silicon breakdown

1. Introduction

With the ATLAS ITk upgrade underway to support the High Luminosity upgrade [1] for the Large Hadron Collider, over 10000 newly developed silicon based sensors [2] have already been produced. These sensors being of a large surface area are prone to occasional failures found during quality control (QC) processing [3, 4] of which the most common is early leakage current breakdown. One step during QC is to record the dependence of the measured leakage current on the applied reverse bias voltage for the sensor (IV Curve). Leakage current is measured up to $-700\ V$, in 10 volts / 10 seconds intervals where the value is on the order of nanoamps/cm^2, and is dependent on the active area, with surface and bulk contributions. According to the ATLAS ITk strip sensor specifications, breakdown cannot occur earlier than $-500\ V$. If breakdown occurs before $-500\ V$, the leakage current typically increases by orders of magnitude, making the sensor unusable as it introduces noise in the readout signals and can prevent the proper biasing of the sensor.

The observation of early breakdown is typically followed by an investigation of the source of the breakdown. Existing procedures involve the use of a microscope to study the surface of the sensor and locate physical damage, such as chipping, scratches, defects discoloration, etc. But once suspect damages are found, the correlation of this damage to the early breakdown is only assumed, and not verified.

Infrared Thermography is sometimes used to observe similar known phenomenon like that of humidity sensitivity [5,6]. In this case, the utilization

of similar hot spot imaging of suspect areas is a valuable tool for the next step of investigations, allowing for the verification of early breakdown locations. Additionally, unexpected results from these studies lead to a better understanding of the nature of early breakdown damage, where breakdown emissions sometime come from unexpected locations. This paper will summarize the procedure and results of hot spot imaging studies on a total of 27 ATLAS18 samples, including full-size sensors and test structures, such as miniature sensors and diodes.

2. Hot Spot Imaging Methodology

2.1. Imaging Hardware and Considerations

Imaging of these early breakdown conditions is notably difficult, requiring a microscopy camera with high quantum efficiency (QE), very low dark current (low thermal noise from the camera sensor), long exposure capabilities, and a reasonable resolution to resolve breakdown details. The Hamamatsu Orca Quest [7] and Teledyne Photometrics Retica E7 [8] fit these requirements. Featuring relatively large 4.6 μm and 4.5 μm pixels with a high resolution sensors, maximum QE of 90 % and 73 %, and -20° C and -25° C cooling respectively, while both supporting 60 minute maximum exposure time.

The expected wavelength of the emissions produced by the breakdown in silicon with a 1.12 eV band-gap can be calculated as:

$$\lambda = \frac{hc}{E_g} = \frac{6.626x10^{-34}\ Js \times 2.998 \times 10^{8}\ \frac{m}{s}}{1.12\ eV \times 1.602 \times 10^{-19}\ \frac{J}{eV}} = 1107\ nm$$

This wavelength is near the far end of the QE capabilities of these cameras as specified by the manufacturers (Figure 1), where sensitivity is very low. Some contribution to the emissions may also come from the bremsstrahlung effect [9], which can create a more broad emission spectrum from silicon, extending in to the visible range. With these spectrum contributions and very long exposure, imaging remains feasible because of the exceptionally low noise performance of the cameras.

The main hardware components of the setup used for breakdown imaging are as follows: Semiprobe PS4L probing station with a dark enclosure and dry atmosphere, Hamamatsu Orca Quest or Teledyne Photometrics Retiga E7 cameras, Keithley 2410 source meter unit (SMU), PSM-1000 Microscope

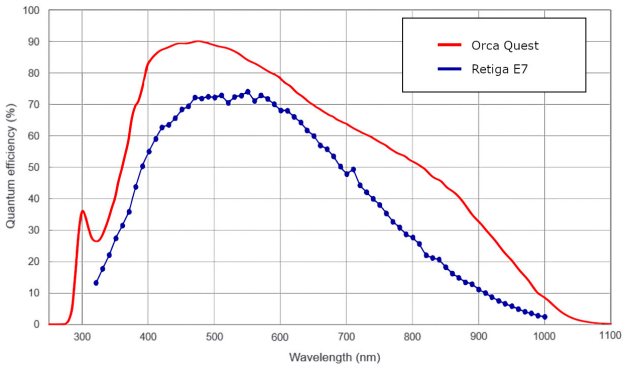

Figure 1: Quantum efficiency of Orca Quest and Retiga E7

with a Motic PLAN APO 2X lens, and finally a Kowa LM25XC 25mm wide angle lens. The imaging configurations are demonstrated in Figure 2: Figure 2A shows the wide angle configuration using the Kowa LM25XC lens and camera attached to the microscope stand via a 3D-printed adapter. Figure 2B shows the Field of View (FOV) of the wide angle lens, covering a surface area of approximately 153 mm x 86 mm. Figure 2C shows the magnified configuration using a microscope with a PLAN APO 2X lens. And, Figure 2D shows the FOV of the magnified image being approximately 9.4 mm x 5.3 mm. The wide angle FOV is slightly smaller on the Retiga E7 as its sensor is lower resolution at 3200 x 2200 compared to the Orca Quest's 4096 x 2304.

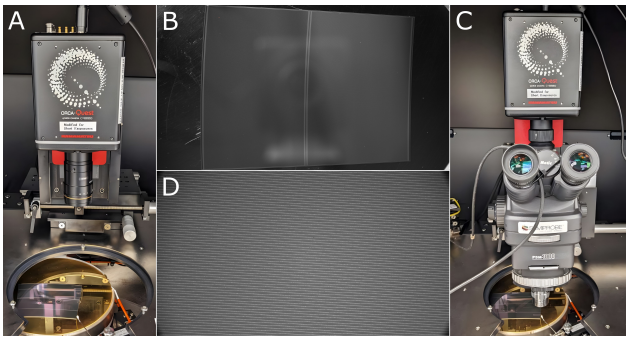

Figure 2: Wide angle imaging setup (left), Wide angle image (top), Magnification setup (right), Magnified image (bottom)

2.2. Imaging and Processing Procedure

The device under test (DUT, see section 3) is first placed on the probing station chuck, and the biasing needle is contacted to the bias ring. The DUT is then moved to be in the full FOV of the camera, and a reference illuminated image is captured. The dark enclosure is then closed and a dry air supply sets the environment to 20 $^{\circ}C$ and under 10 % relative humidity. The KE2410 SMU is then enabled, and the voltage is ramped up until breakdown has occurred and current has reached over roughly 5 μA where emissions may be visible. Various emission captures are then attempted, using various exposure times ranging from 5 to 480 seconds (typically 10 to 60 seconds was sufficient to find the breakdown). Once a region of interest (ROI) is found, the DUT is unbiased, then the camera is moved to the 2X microscope and the ROI is located. The steps above are then repeated to capture magnified images of the emissions.

Figure 3 shows the data processing work flow using GIMP (GNU Image Manipulation Program). The procedure is as follows:
Figure 3A) An illuminated image is taken as the reference for breakdown positioning. Lighting is then turned off, dry air is enabled, and bias voltage is ramped up to a level where a sufficient magnitude of current is present for emissions to appear.
Figure 3B) The captured emission is contrast stretched to bring out the data (Range from darkest to brightest pixels stretched to minimum and maximum 12 bit values).
Figure 3C) The background is removed by means of levels adjustments and dark image subtractions, the resulting image is then colorized.
Figure 3D) Finally the emission image is overlaid as a screen on the illuminated reference image.
These processing steps are taken for every sample, and sometimes multiple exposures are superimposed with various colors.

2.3. Imaging Requirements, Limitations, and Performance

The primary requirement for imaging was found to be the amount of current flow. The current required is often related to the type of damage; if the damage area is large, the current required to get emission levels above the noise floor is higher; if the damage area is a pinpoint, it will typically be visible at lower current levels. This required level typically falls on the order of micro amps, and most imaging was done with between 5 and 45 μA, and most of the time on the higher side of that range. Lower current

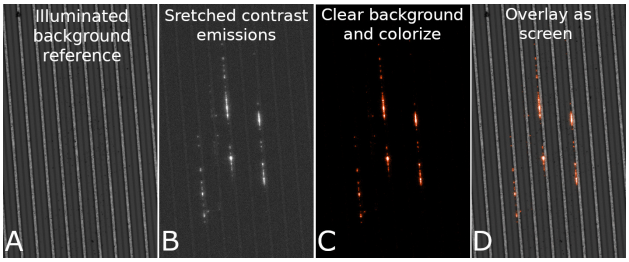

Figure 3: Data processing procedure using Retiga E7 captures and GIMP

levels may also only show a limited section of the breakdown area, where with higher current the initial area will become brighter, larger, or new areas may emerge, a phenomenon that will be a subject of further studies.

The shape and nature of the breakdown curve also notably impacts the brightness of emissions produced. Figure 4 has three examples of common breakdown curves. "Normal Early Breakdown" starts at a low current and then has a distinct spike in the rate of increase in of leakage current, this type of breakdown is often easily imaged. "Soft Breakdown" is when the rate of increase in current rises consistently throughout the whole voltage range, and "Instant Breakdown" is when the rate of increase in current starts high and remains high throughout the voltage range. "Soft" and "Instant" breakdown are often very difficult to image since the damage area is likely quite large, additionally the emissions may be further in to the infrared where the cameras are not sensitive.

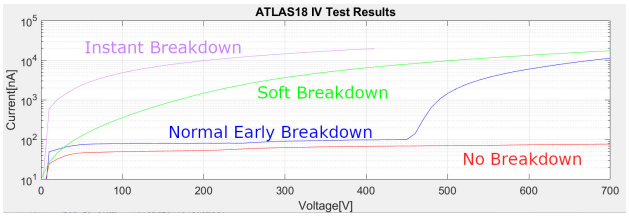

Figure 4: Typical IV breakdown behaviors

An additional challenge while capturing emissions is that of light transmission. The Kowa LM25XC has a visible and broadband coating for near infra-red (NIR) which allows approximately 50% light transmission at 1100nm wavelength. The microscope's Motic PLAN APO 2X lens on the other hand is coated only for the visible spectrum, with much lower transmission of NIR.

Therefore some emissions were much easier to capture using the wide angle lens, and when observed at magnification they required an order of magnitude longer exposure time to capture. The Retiga E7 featured a 2x1 hybrid binning system that could be used to increase sensitivity at the expense of resolution, which proved useful to capture the most challenging emissions through the non-ideal microscope lens. Some emissions were also dynamic, changing location over time, therefore requiring multiple captures to fully characterize the breakdown.

3. Devices Under Test

The devices used consist of components on wafers for the ATLAS18 ITk endcap production sensors [2]. These are fabricated by Hamamatsu on 6 inch wafers, with the main strip sensor in the center. The outer areas around the center (Halfmoons) feature various test structures including miniature strip sensors and diodes which were used in these investigations. The full size sensor samples chosen are found during quality control, where they are investigated because of early breakdown. The halfmoons are used for intentional damage studies, where various tools are used to inflict damage and induce breakdown for imaging studies.

All devices featured are biased using the backplane and a n-implant bias ring surrounding the perimeter of the active area. This is followed by one n-implant guard ring and one p-implant edge ring that are often correlated with early breakdown caused by edge damage. Strips with open aluminum AC pads are separated from adjacent strips with p-stop, and covered with a passivation layer for protection. Diode test structures are typically un-diced and tested on the halfmoons and are either 2, 4, or 8 mm wide square areas following a similar structure with a bias ring followed by a guard and edge rings surrounding the interior active area.

4. Results, Failure Mode Analysis From Emissions

4.1. Scratches and Punctures

Many earlier samples were created using intentional damage on the test structures on the halfmoons of wafers. Figure 5 shows multiple examples of diodes of various sizes producing emissions from intentional damage using a tungsten carbide scribe tip. Figure 5A-5D are scratches in different locations

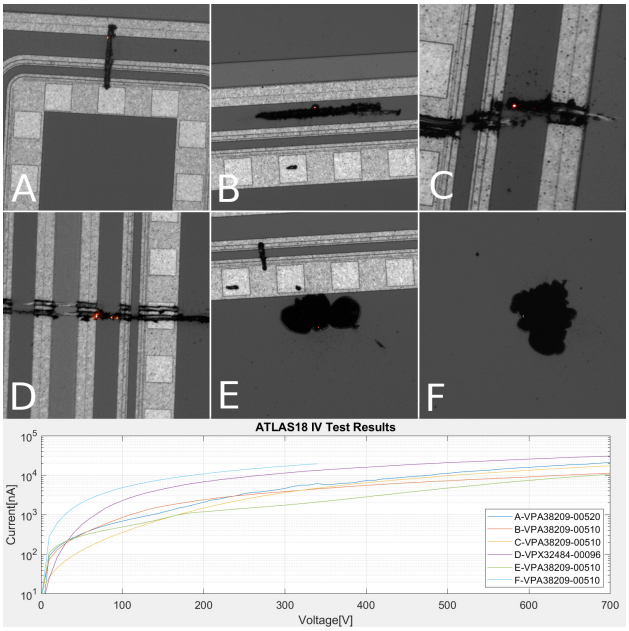

Figure 5: Several examples of intentional scratch damage emissions highlighted in red, IV's at the bottom

which caused emissions clearly imaged usually taken at over 20 μA and 60-240 seconds of exposure. The current and exposure times are high on these samples due to the either soft or instant breakdown (bottom of Figure 5). These scratches typically produce emissions from within the scratch so long as the damage is between the bias, guard and edge rings, and especially bright emissions when the scratch bridges them. Images E and F are damages caused by pressing the tungsten carbide scribe in to the surface of the active area, this made a large dark area where breakdown emissions is visible on the edge. In these tests, it was also found that too much damage would create instant breakdown with emissions that were difficult to or could not be captured, as explained in section 2.3.

4.2. Chipping and Defects

The most common failure mode is that of edge chipping. Often, if a chip on the edge reaches the metal of the edge ring, usually over 100 μm from the silicon edge, normal early breakdown will occur (bottom of Figure 6). Figure 6A shows one of these examples, where breakdown emissions appeared in close proximity to a chip reaching well past the edge ring. Figure 6D shows

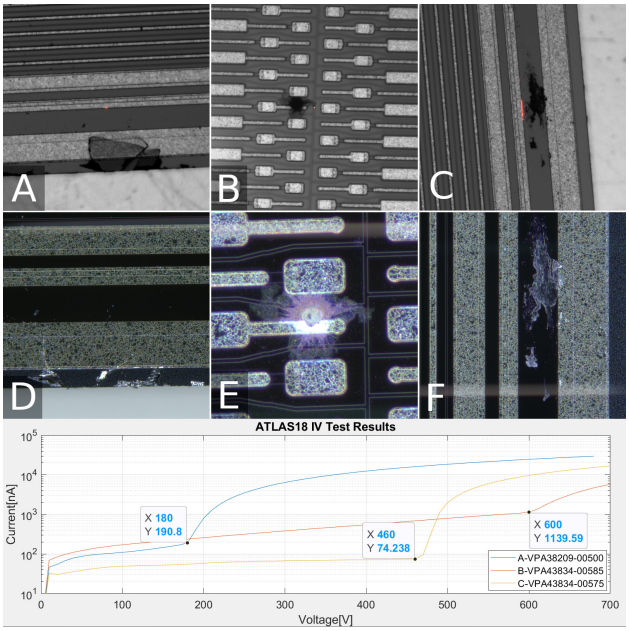

Figure 6: A-C) Emissions from chips and defects, D-F) Color microscope images of the damaged areas, IV's at the bottom

deep chipping on the edge. Defects also occur like that shown in Figure 6B and 6C which exhibit similar breakdown behavior. Figure 6B shows emissions occurring near a dark spot in the active area, where a defect meets the p-stop. Figure 6E shows the embedded defect in more detail, with it reaching from the strip to the p-stop area. This sample was of interest because the DUT also had significant chipping damage on the edge which was thought to be the source of early breakdown, proven wrong by the identification of this defect via hot spot imaging. Finally, Figure 6C shows a contaminant between the guard ring and edge ring, with the emissions occurring along the guard ring and closest to the contaminant. Figure 6F shows this contaminant in more detail, it may interfere with the edge structure performance.

4.3. Passivation damage

One of the most interesting failure modes was that of apparent passivation layer damage. These emission regions tend to be much larger in size than other examples, and are partially dynamic in nature. Figure 7A - 7C show three examples of this type of damage taken at 34, 20 and 20 μA of current respectively with initial IV curves of these samples being normal early

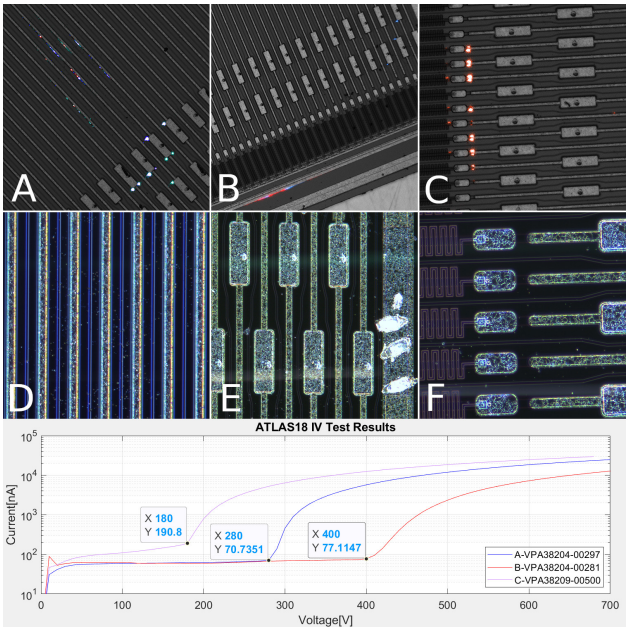

Figure 7: A-C) Three examples of emissions from suspected passivation layer damage from bad wire bond placements D-F) Color microscope imaging showing a speckling in the regions nearby emissions, IV's at the bottom

breakdown (bottom of Figure 7). Figure 7A and 7B have multiple colors demonstrating captures taken with a pause of roughly 5 minutes with the DUT left biased. If the bias is left on and given time, the emissions will actively change position within the region of the damage. Figure 7A was the most dynamic region, where the three different colored emissions have several areas without overlap with other emissions.

This type of emission appears to be correlated with a possible damage source and damage appearance which is visible in all three Figure 7D - 7F. The suspected damage source present on all three samples is that of the bad wire bond placement shown in Figure 7E, where the wire bond foot reaches in to the active area. It is suspected that this caused damage to the passivation layer in the active area, which shows itself physically as the speckling between features clearly visible in Figure 7D - 7F. This wirebond placement issue was corrected in production flow as a result of these investigations.

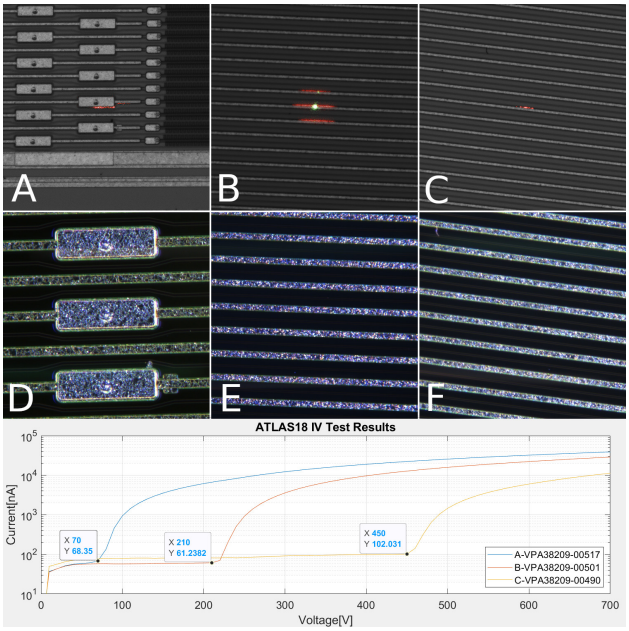

Figure 8: A-C) Emissions created by trapped static charge D-F) Color microscope images showing no physical damage in the area, IV's at the bottom

4.4. Static charge

Another intriguing case of emissions came in the form of not being correlated with any visible physical damage, yet exhibiting normal early breakdown like many other samples (bottom of Figure 8). Instead, these emissions would appear sometimes near the AC pads, as shown in Figure 8A, and sometimes near strips in the active area like that of Figure 8B and 8C. Color microscope captures Figure 8D - 8F show no signs of physical damage in the breakdown areas. It was later found that this was the result of trapped static charge changing the properties of the materials around the strips resulting in loss of isolation between components. It was also found that this type of damage could be cured with 400 nm UV light exposure or with deionizers [10][11]. Figure 8B shows the original emissions found in red where breakdown started at $-210\ V$, as well as post 1 hour UV treatment in yellow where breakdown now started at $-790\ V$ instead and the emissions region was much smaller. Figure 8C is yet another example of this phenomenon, similar to Figure 8B, breakdown is happening on the edge of a strip with no obvious damage. It was found that with additional UV exposure time, approximately 4 hours using two 100 W 400 nm UV LED's, all three of these

examples were repaired and no longer broke down before -1 kV.

5. Conclusions

Using the equipment and procedures outlined in this paper, 27 samples from ATLAS18 production sensors and halfmoon test structures were examined. Of these 27 samples, 14 were intentional damage where 10 samples had successful emission captures, and 13 were full size production sensors where 10 samples had successful emission captures. This demonstrated that the equipment utilized performed well in this application, allowing proper diagnostics of various breakdown emission types.

Various characterizations of breakdown behaviors were also successfully verified and documented including scratching, chipping, defects, passivation damage, and trapped static charge. Of these behaviors, defects, passivation damage and trapped static charge proved the most interesting. Sometimes defects proved to be the actual source of early breakdown contrary to other identified physical damage. Other times, the damage was not physical nor permanent and was found to be trapped static charge that could be repaired with UV light exposure. It was also found that breakdown emissions can be dynamic, and will change position depending on leakage current and time. And finally, some damage was found to be related to bad wirebond placement resulting in passivation layer damage and production flow changes to avoid future cases of this damage.

A better understanding of hot spot imaging limitations was established. Some expected parameters were found that proved integral to the probability of emissions being captured. These limitations included breakdown type, minimum leakage current, and breakdown area size, all of which contribute to the magnitude of emissions available. Additional studies are planned to elaborate on these emissions limitations and to perform additional diagnostics and characterizations.

Acknowledgements

This work is part of the Spanish R&D grant PID2021-126327OB-C22, funded by MCIN/ AEI/10.13039/501100011033 / FEDER, UE. The work at SCIPP was supported by the US Department of Energy, grant DE-SC0010107. This work was supported by the Canada Foundation for Innovation and the

Natural Sciences and Engineering Research Council of Canada.

References

[1] L. Rossi, et al., Technical Report, CERN, Geneva, 2012. URL: https://cds.cern.ch/record/1471000.

[2] Y. Unno, et al., JINST 18 (2023) T03008. URL: https://doi.org/10.1088/1748-0221/18/03/T03008.

[3] M. Mikestikova, et al., JINST 17 (2022) C12013. URL: https://dx.doi.org/10.1088/1748-0221/17/12/C12013.

[4] D. Rousso, et al., NIM A 1045 (2023) 167608. URL: https://doi.org/10.1016/j.nima.2022.167608.

[5] J. Fernández-Tejero, et al., NIM A 978 (2020) 164406. URL: https://doi.org/10.1016/j.nima.2020.164406.

[6] J. Fernández-Tejero, UAB, Ph.D. thesis, 2020. URL: https://jinst.sissa.it/jinst/theses/2020_JINST_TH_004.jsp.

[7] Hamamatsu, Orca-quest, 2022. URL: https://www.hamamatsu.com/jp/en/product/cameras/qcmos-cameras/C15550-20UP.html.

[8] Teledyne-Photometrics, Retiga e7, 2023. URL: https://www.photometrics.com/products/retiga-e-family/retiga-e7-cmos.

[9] N. Akil, et al., IEEE Transactions on Electron Devices 46 (1999) 1022–1028. URL: https://doi.org/10.1109/16.760412.

[10] E. Staats, et al., NIM A submitted for publication (2023). URL: https://cds.cern.ch/record/2882291.

[11] P. Federičová, et al., JINST 19 (2024) C02001. URL: https://dx.doi.org/10.1088/1748-0221/19/02/C02001.